

We are IntechOpen, the world's leading publisher of Open Access books Built by scientists, for scientists

6,900

Open access books available

186,000

International authors and editors

200M

Downloads

Our authors are among the

154

Countries delivered to

TOP 1%

most cited scientists

12.2%

Contributors from top 500 universities



WEB OF SCIENCE™

Selection of our books indexed in the Book Citation Index
in Web of Science™ Core Collection (BKCI)

Interested in publishing with us?
Contact book.department@intechopen.com

Numbers displayed above are based on latest data collected.
For more information visit www.intechopen.com



Minimalist Approach for the Design of Microstructured Optical Fiber Sensors

Jonas H. Osório and Cristiano M. B. Cordeiro

Abstract

We report on recent investigations regarding ultra-simplified designs for microstructured optical fiber sensors. This minimalist approach relies on the utilization of capillary-like fibers—namely embedded-core fibers, surface-core fibers, and capillary fibers—as platforms for the realization of sensing measurements. In these fibers, guidance of light is accomplished in an embedded or surface germanium-doped core or in the hollow part of capillaries. External stimuli can alter fiber wall thickness and/or induce birefringence variations, allowing, for the embedded-core and capillary fibers, to operate as pressure or temperature sensors. For the surface-core fiber design, the interaction between the guided mode and external medium allows the realization of refractive index sensing either by using fiber Bragg gratings or surface plasmon resonance phenomenon. Also, we report the realization of directional curvature sensing with surface-core fibers making use of the off-center core position. The attained sensitivities are comparable to the ones obtained with much more sophisticated structures. The results demonstrate that these novel geometries enable a new route toward the simplification of optical fiber sensors.

Keywords: fiber optics, fiber optics sensors, fiber Bragg gratings, surface plasmon resonance, microstructured optical fibers

1. Introduction

The increasing need for the development of optical sensors motivates intense research in this area. Particularly, great efforts have been observed in the field of optical fiber sensors since they can provide numerous advantages such as high sensitivity and improved resolution. Moreover, fiber optics are immune to electromagnetic interference and suitable to be used in harsh environments.

In this context, microstructured optical fibers have much contributed to the development of sensors due to their huge design freedom. Thus, numerous sensing configurations have been reported in the literature to be able to probe variations of a great diversity of parameters such as temperature, strain, hydrostatic pressure, curvature, and refractive index. Regarding pressure sensors, for example, successful approaches are to use photonic-crystal fibers (PCFs) with triangular-shaped microstructures [1] or side-hole PCFs [2]. In these configurations, the hydrostatic pressure application generates asymmetric stresses distributions within the fiber

structure and changes its birefringence via the photoelastic effect. Additionally, metal-filled side-hole PCFs have been demonstrated to act as high-sensitivity temperature sensors [3, 4]. In this approach, the metal expansion inside the fiber structure induces an asymmetric stress distribution within the same (due to the different thermal expansion coefficients of silica and of the metal). It entails changes in the fiber birefringence which can be optically probed and related to the temperature variation through a suitable calibration.

Microstructured optical fibers can also be used as refractive index sensors. Among those ones, plasmonic sensors acquire great importance due to the high sensitivities they can achieve. In these platforms, selected regions of the fiber structure are coated with a nanometric-thick metallic layer to provide coupling between the optical mode and a plasmonic mode. Possible approaches are to coat the inner holes of microstructured fibers [5] or to open up a channel in the fiber structure to expose the fiber core for metallic nanospheres immobilization [6].

However, the microstructured optical fibers usually employed in the sensing schemes described above are sophisticated, which demand great technical efforts for their fabrication. Here, alternatively, we present sensors which are endowed with ultra-simplified microstructures based on capillary-like fibers (embedded-core fibers [7, 8], surface-core fibers [9, 10], and capillary fibers [11]). As it will be shown in the following, even though these configurations are very simple, the attained sensitivities are high when compared to other fiber sensors based on more complex structures. Thus, we can identify the use of capillary-like fibers as a new avenue for obtaining highly sensitive fiber sensors with simplified fabrication process.

2. Capillary-like fiber designs for sensing applications

Figure 1 shows the fiber designs we present here. In **Figure 1a**, a diagram of the embedded-core fiber is shown [7, 8]. This structure consists of a silica capillary endowed with a germanium-doped core, which is placed inside the wall of the capillary. The embedded-core fiber can be employed for pressure or temperature sensing measurements. Specifically, when the embedded-core fiber acts as a temperature sensor, the capillary hollow part must be filled with metal (**Figure 1b**). The principle of operation of these sensors is centered on the capillary wall displacements that occur when the hollow embedded-core fiber is pressurized or when the metal-filled embedded-core fiber experiences temperature variations. These wall displacements within the capillary wall entail asymmetric stress distributions in the

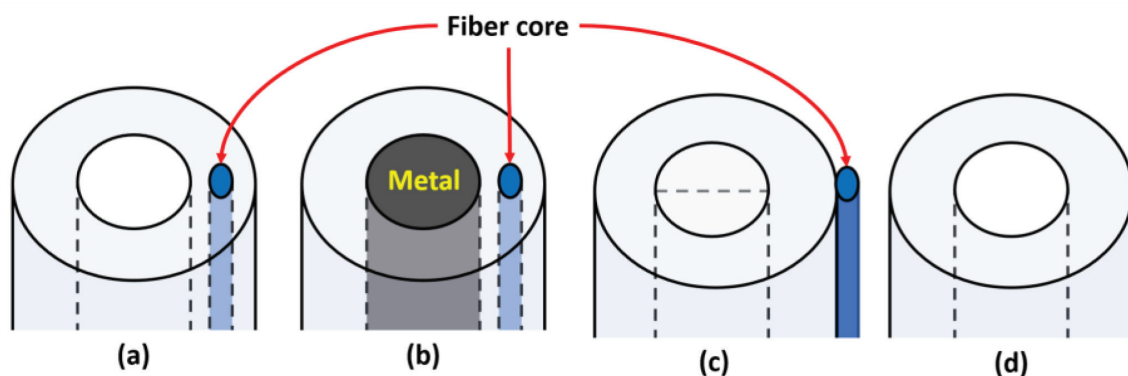


Figure 1.
 (a) Embedded-core fiber, (b) metal-filled embedded-core fiber, (c) surface-core fiber and (d) capillary fiber.

fiber structures, which generate, by virtue of the photoelastic effect, birefringence variations in the fiber core.

Figure 1c shows a diagram of the so-called surface-core fiber [9]. In this structure, the fiber core is placed on the fiber external surface. As here the core directly interfaces the external medium, the evanescent field of the guided optical mode permeates the external environment. Surface-core fibers are, then, a suitable platform for refractive index sensing. A possible approach is to imprint fiber Bragg gratings (FBGs) in the fiber core and measure the sensor spectral response as the external refractive index is altered [9]. A second approach is to perform plasmonic sensing by metal-coating the surface-core fiber with a nanometric metallic layer [10]. Additionally, the off-center position of the fiber core permits the surface-core fibers to act as directional curvature sensors. In this case, the curvature-induced strain levels within the core can be probed by a FBG [9].

Figure 1d presents a fourth structure, which is simply a capillary fiber [12]. Here, we study the guidance of light in the hollow part of the capillary and investigate how the optical response of the fiber is changed when it experiences temperature variations. It is worth saying that, in this investigation, we employed polymethyl methacrylate (PMMA) capillaries. This choice was due to the higher thermal expansion and thermo-optic coefficients of PMMA when compared to silica.

In the next sections, we specifically describe the principle of operation of each configuration. Moreover, we present theoretical and experimental results and compare them with the ones available in the literature.

3. Embedded-core capillary fibers for pressure sensing

The application of pressure to capillary fibers generates displacements on their walls. This, in turn, induces an asymmetric stress distribution within the capillary structure which, due to the stress-optic effect, entails birefringence variations in it. As described in [7], an analytical model can be used to account for the material birefringence variations (ΔB_{mat}) in pressurized capillaries. To do that, we can employ Eq. (1), where C_1 and C_2 are the elasto-optic coefficients ($C_1 = -0.69 \times 10^{-12}$ and $C_2 = -4.19 \times 10^{-12} \text{ Pa}^{-1}$ for silica), and σ_x and σ_y are the pressure-induced stresses on the horizontal and vertical directions, respectively [13, 14].

$$\Delta B_{mat} = (C_2 - C_1)(\sigma_x - \sigma_y) \quad (1)$$

The stresses σ_x and σ_y can be obtained from Lamé solution inside thick-walled tubes subjected to pressure [15]. The resulting expression for the material birefringence at a position x on the horizontal axis is shown in Eq. (2), where r_{in} and r_{out} are the inner and outer radius of the capillary, and $p_{gauge} = p_{out} - p_{in}$ (p_{in} and p_{out} are the inner and outer pressure levels) [7].

$$\Delta B_{mat} = 2(C_2 - C_1)p_{gauge} \left[1 - \left(\frac{r_{in}}{r_{out}} \right)^2 \right]^{-1} \frac{r_{in}^2}{x^2} \quad (2)$$

By observing Eq. (2), we see that, when maintaining r_{in} constant, $|\Delta B_{mat}|$ will be greater for higher r_{in}/r_{out} ratios. It means that the analytical model predicts that the change in the birefringence is increased for thin-walled capillaries. Moreover, we see that, for fixed r_{in} and r_{out} values, the change in the birefringence is higher for positions (x) which are closer to the inner wall of the capillary [7].

Although the analytical model for the material birefringence can provide important information on the most important geometrical parameters that affects the sensitivity of the sensor, it is necessary to account for the modal birefringence dependence on the applied pressure for a broader understanding of the sensor characteristics. To do this, a numerical simulation of the embedded-core fiber structure was carried on. **Figure 2** presents the results for dB_{modal}/dP (derivative of the modal birefringence as a function of the pressure) as a function of the core position within the capillary. In the simulations, $r_{\text{in}} = 40 \mu\text{m}$ and $r_{\text{out}} = 67.5 \mu\text{m}$. The core dimensions were considered to be 5.7 and $11.4 \mu\text{m}$.

The results presented in **Figure 2** show, as could be expected from the analytical model, that dB_{modal}/dP values are higher for core positions which are closer to the inner wall of the capillary. However, we note that, very interestingly, the trend that is expected from the analytical model is verified only when the whole core is within the capillary wall. When the core has part of its area outside of the capillary wall, a strong decrease in dB_{modal}/dP is observed (core region is represented as dark blue ellipses in **Figure 2**). This allows observing that, for maximizing dB_{modal}/dP in embedded-core fibers, it is crucial that the whole core is inside the capillary wall.

In order to obtain an experimental demonstration of the proposed design acting as a pressure sensor, we performed the fabrication of the embedded-core fiber. The fabrication process is simple and with few steps. Initially, a germanium-doped silica rod is merged to a silica tube. In sequence, the resulting preform is inserted in another silica tube, which acts as a jacket. The preform is then drawn in a fiber tower facility [7]. **Figure 3a** shows the cross-section of the embedded-core fiber.

Figure 3b exposes a diagram of the experimental setup used for pressure measurements. Light from a broadband source (BLS) is launched in the fiber and detected with an optical spectrum analyzer (OSA). Polarizers (P_1 and P_2) are used to excite the orthogonal modes of the fiber and to recombine them after traveling along the fiber. A pressure chamber is used to subject the fiber to different pressure levels.

By using the configuration of **Figure 3b**, an interference spectrum is measured in the OSA. Since the embedded-core fiber is sensitive to pressure variations, the spectral position of the interferometric fringes is shifted when the external pressure level is altered. A sensitivity coefficient, C_S , is defined to account for the spectral shift of the fringes as a function of the pressure variation, $\frac{d\lambda_F}{dP}$. The C_S value can also be written as a function of the wavelength, λ , the fiber group birefringence, G , and

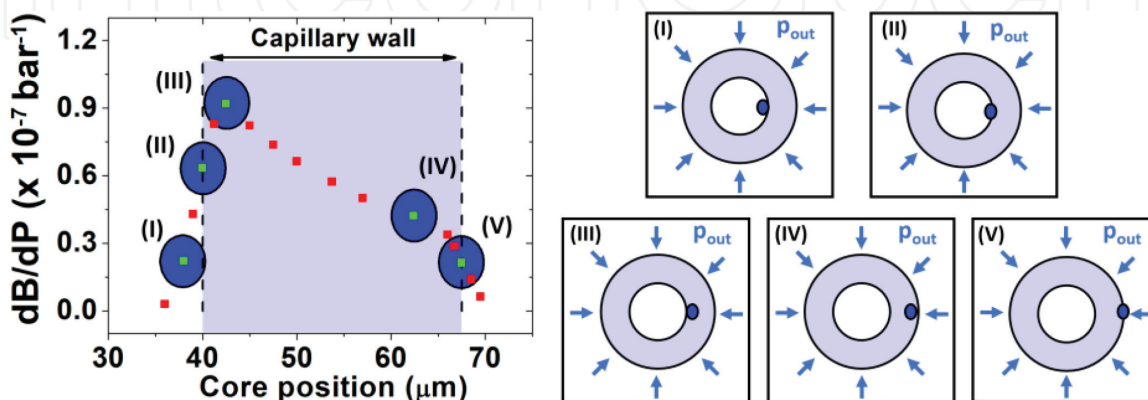


Figure 2. Modal birefringence derivative as a function of pressure for different core positions inside the capillary wall. Light blue region represents the capillary wall, and dark blue ellipses represent the core region. Insets illustrate the core position within the capillary.

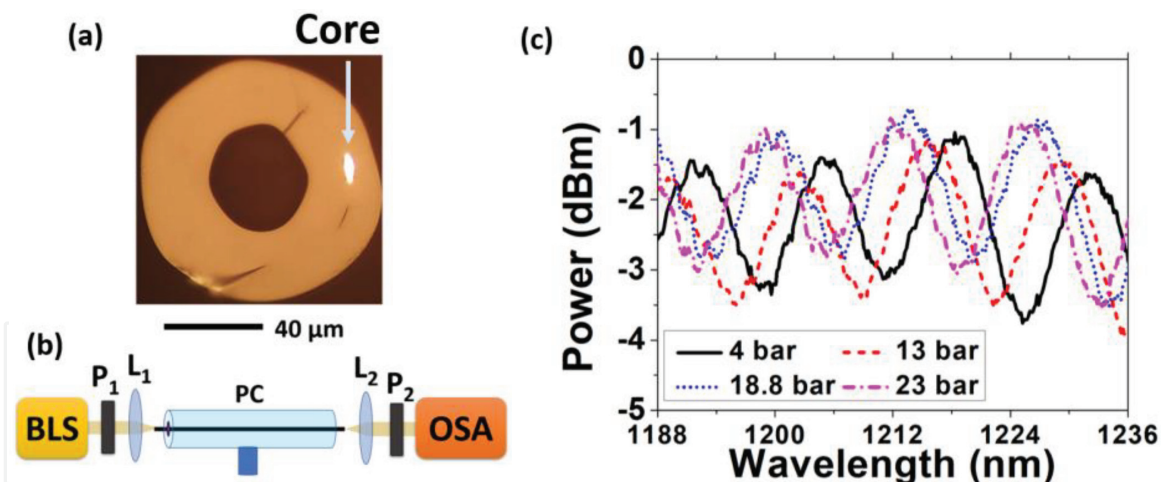


Figure 3. (a) Embedded-core fiber. (b) Experimental setup for pressure sensing measurements. BLS: broadband light source. P_1 and P_2 : polarizers. L_1 and L_2 : objective lenses. PC: pressure chamber. (c) Spectral response of the embedded-core fiber for different pressure levels.

of the modal phase birefringence derivative with respect to the pressure, $\frac{\partial B_{\text{modal}}}{\partial P}$ — Eq. (3) [2].

$$C_s \equiv \frac{d\lambda_{\text{IF}}}{dP} = \frac{\lambda}{G} \frac{\partial B_{\text{modal}}}{\partial P} \quad (3)$$

Figure 3c presents the measured optical response of the embedded-core fiber for different pressurization conditions. It is seen that when the pressure level increases, the fringes blueshift. After performing an appropriate correction on the fiber pressurized and nonpressurized lengths [2, 16], we can estimate a sensitivity value of (1.04 ± 0.01) nm/bar [7]. This value is high when compared to other results measured in polarimetric measurements reported in the literature. For example, in [17], a sensitivity of 0.342 nm/bar was measured for a commercial photonic-crystal fiber. Additionally, in [18, 19], the sensitivities of 0.30 and 0.52 nm/bar were reported for specially designed microstructured fibers.

Moreover, the $\frac{\partial B_{\text{modal}}}{\partial P}$ value for the embedded-core fiber can be estimated from Eq. (3). The resulting value is $(2.33 \pm 0.02) \times 10^{-7} \text{ bar}^{-1}$, which is in the same magnitude order of the ones found for much more sophisticated microstructured fibers [1]. Therefore, we see that the embedded-core fiber structure allows achieving high sensitivity (C_s) and $\frac{\partial B_{\text{modal}}}{\partial P}$ even with a nonoptimized fiber. It also allows recognizing embedded-core fiber as a promising platform for the realization of pressure sensing using optical fibers and a novel route for the design of microstructured optical fiber pressure sensors.

4. Embedded-core capillary fibers for temperature sensing

Embedded-core fibers can also act as highly sensitive temperature sensors if a metal is inserted into the hollow part of the capillary (**Figure 1b**). In analogy to the embedded-core fiber pressure sensor, the principle of operation is based on the induction of stresses inside the capillary and on the consequent variation of the fiber birefringence [8].

In this configuration, the metal expansion inside the capillary causes its volume elements to displace and to compress the silica capillary structure. This, in turn,

entails an asymmetric stress distribution within the capillary wall and induces birefringence variations. An analytical model can be used to predict the most relevant parameters that contribute to the sensor response. This analytical model provides Eq. (4), which accounts for the variation in the material birefringence of the capillary, ΔB_{mat} , for a given temperature variation, ΔT (r_{in} and r_{out} are the capillary inner and outer radii, and C_1 and C_2 are the silica elasto-optic coefficients). The parameter δ in Eq. (4) is given by Eq. (5), where ν is the Poisson ratio, E is the Young modulus, and α is the thermal expansion coefficient. In Eq. (5), index 1 refers to the filling metal and index 2 refers to silica [8]. By observing Eq. (4) and Eq. (5), it is possible to realize that $|\Delta B_{mat}|$ will be greater for positions closer to the inner radius and when the filling metal has a larger thermal expansion coefficient.

$$\Delta B_{mat} = -2\delta\Delta T(C_2 - C_1)\frac{r_{out}^2}{x^2} \quad (4)$$

$$\delta = \frac{(1 + \nu_2)\alpha_2 - (1 + \nu_1)\alpha_1}{\frac{(1+\nu_1)}{E_1}\left(\nu_1 - \frac{1}{2}\right) + \frac{(1+\nu_2)}{E_2}\left(\nu_2 - \frac{1}{2} - \frac{r_{out}^2}{r_{in}^2}\right)} \quad (5)$$

Thus, indium was chosen to be the filling metal due to its high thermal expansion coefficient ($32.1 \times 10^{-6}\text{°C}^{-1}$) and reasonably low melting point (156°C) [3]. The low melting point is an important property since it simplifies the metal filling process. To insert the metal inside the embedded-core fiber, the metal is molten and pressure is applied to push it into the hollow region.

Figure 4a shows the indium-filled embedded-core fiber. To measure its temperature sensitivity, the same experimental setup as represented in **Figure 3b** was used. The unique difference is that, for the temperature sensing measurements, the pressure chamber was substituted by a water reservoir placed on a hot plate in order to adequately alter the fiber temperature.

Figure 4b shows the spectra measured for different temperature conditions. We see that there is a spectral shift toward longer wavelengths as the temperature is increased. After performing a suitable correction on the heated and unheated fiber lengths, the sensitivity was calculated to be $(8.40 \pm 0.06) \text{ nm/°C}$ [8]. This sensitivity value compares well to the highest temperature sensitivity values reported in the literature such as 9.0 [4], 6.6 [20], and 16.49 nm/°C [21], which were measured for photonic-crystal fibers filled with indium, ethanol, and index matching liquid, respectively. This once again demonstrates that embedded-core fibers are a very promising platform for the realization of high-sensitivity optical sensing.

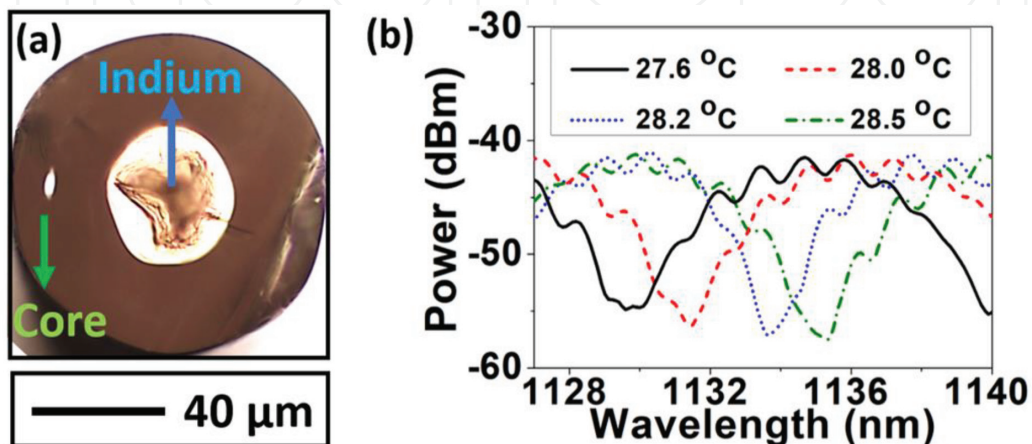


Figure 4. (a) Indium-filled embedded-core fiber. (b) Spectral response of the indium-filled embedded-core fiber for different temperature conditions.

5. Surface-core fibers for refractive index sensing

A third sensing opportunity under the approach of simplified optical fiber sensors is the employment of surface-core fibers [9]. In this kind of fibers, the core is placed on the outer surface of the same (Figure 1c). The proximity of the core to the external environment makes surface-core fibers suitable to be used as refractive index sensors, and the off-center position of the core allows these fibers to operate as directional curvature sensors. Figure 5a presents the cross-section of the surface-core fiber.

In order to explore the refractive index sensitivity of surface core fibers, fiber Bragg gratings (FBGs) can be inscribed in the fiber core [9]. FBGs consist of a refractive index modulation in the core of the fiber able to couple the propagating core mode to a contra-propagating one. The coupling between the modes is achieved at a specific wavelength, λ_B , which can be accounted by Eq. (6), where n_{eff} is the effective refractive index of the core mode and Λ is the pitch of the grating. Experimentally, the response of FBGs is seen as a reflection peak at λ_B .

$$\lambda_B = 2n_{eff}\Lambda \quad (6)$$

As the optical mode guided in the core directly interfaces the external medium, the effective refractive index of the core mode will be dependent on the external refractive index variations. Thus, if the refractive index of the external environment is altered, a shift in the spectral position of the Bragg peak is expected.

Figure 5b presents the measured wavelength shift of the Bragg peak as a function of the external refractive index. As can be seen in Figure 5b, the results for the surface-core fiber showed low sensitivity. To improve the sensor response, tapers from the surface-core fiber were prepared prior to grating inscription. By doing this, it is possible to enhance the interaction between the guided mode evanescent

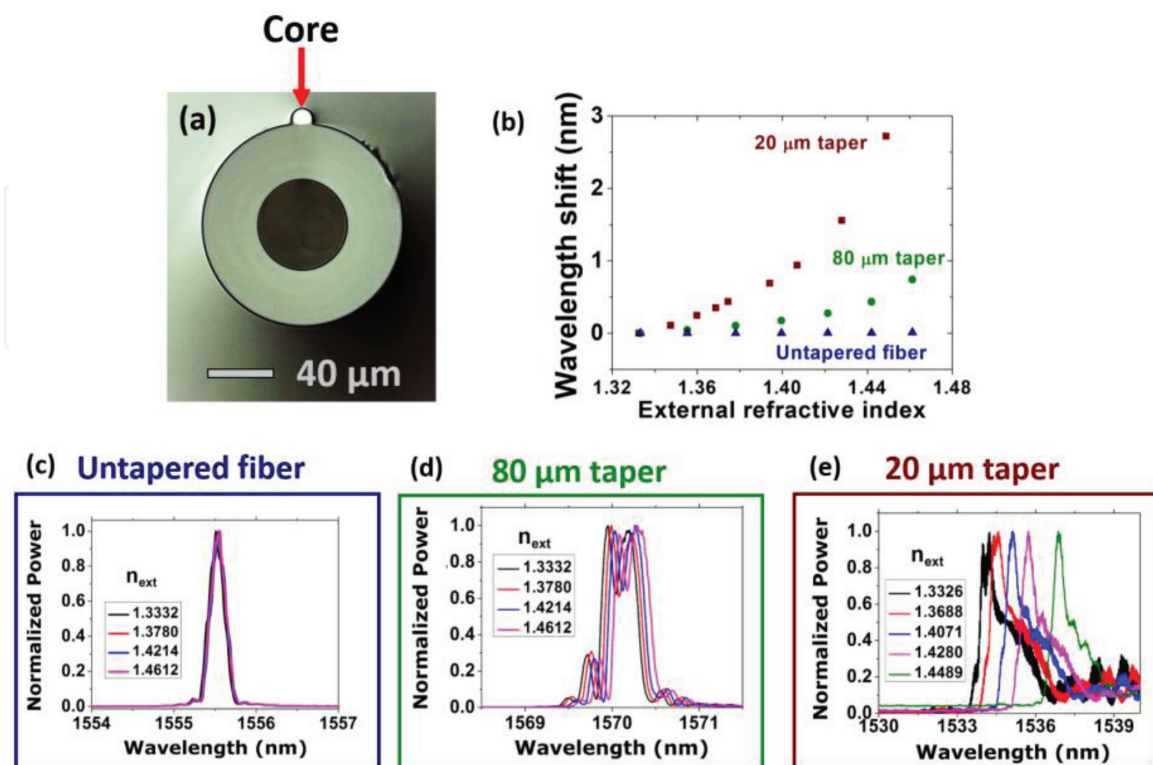


Figure 5. (a) Surface-core fiber. (b) Wavelength shift of the Bragg peak as a function of the external refractive index. Reflected Bragg peaks in the (c) untapered surface-core fiber and in the (d) 80 μm and (e) 20 μm tapers.

field and the external medium and improve the sensitivity. The results measured for tapers with 80 and 20 μm diameter are also shown in **Figure 5b**. The Bragg peaks for the untapered surface-core and for the 80 and 20 μm tapers are shown in **Figure 5c–e**—the gratings were imprinted via phase-mask technique by employing phase masks with pitches 1075.34 nm (for the 80 μm taper) and 1071.2 nm (for the untapered fiber and for the 20 μm taper). Around 1.42 RIU (refractive index unit), the measured sensitivities were 8 and 40 nm/RIU for the 80 and 20 μm tapers, respectively. These sensitivity values compare well with other results for FBG-based refractive index sensors. In [22], it is reported a sensitivity of 15 nm/RIU for a Bragg grating inscribed in a 6- μm -thick taper (measured around 1.326 and 1.378 RIU) and, in [23], a sensitivity of 30 nm/RIU was measured for a 8.5- μm taper (in the same refractive index range). It is worth observing that the results for surface-core fibers were attained for thicker tapers, which implies in sensor robustness improvement.

Another possibility for exploring the sensitivity of surface-core fibers to variations in the refractive index of the external medium is to functionalize the core with a metallic nanolayer and make the fiber to act as a plasmonic sensor. In this approach, the core mode can be resonantly coupled to a plasmonic mode when phase-matching occurs between them (surface plasmon resonance—SPR). The coupling between these modes is seen as a spectral dip at the wavelength where the phase matching condition is achieved. As the fiber core directly interfaces the external medium, the spectral position of the plasmonic resonance will be dependent on the refractive index of the external environment. The sensitivity of the configuration is, therefore, accounted from the spectral shift of the plasmonic resonance as a function of the external refractive index variation.

Figure 6a presents a simulation on the transmittance of the surface-core fiber plasmonic sensor for different refractive index values. In the simulations, the fiber core is assumed to have a 10 μm diameter and to be coated with a gold layer of 50 nm thick. It is seen that the plasmonic resonance is shifted toward longer wavelengths as the external refractive index increases. The sensitivity accounted from the simulations is 1290 nm/RIU. In addition, in **Figure 6b**, the core mode intensity profiles are shown when it is not phase-matched (off-resonance) and when it is phase-matched (in resonance) with the plasmonic mode. We can observe that, when the modes are in resonance, they hybridize. The intensity profiles in **Figure 6b** were calculated for an external refractive index of 1.39. The phase-matched intensity profile was accounted at 600 nm and the one for the off-resonance condition was accounted at 720 nm.

To experimentally test the proposed sensor, the fiber core was coated with a gold layer of 50 nm thick, and sensing measurements were performed at the Aalto

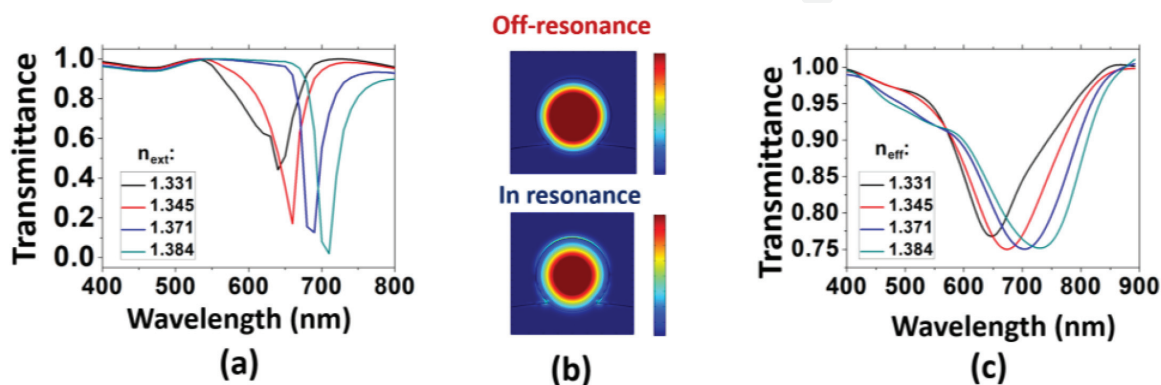


Figure 6.

(a) Simulated transmittance for different external refractive indexes (n_{ext}). (b) Intensity profiles of the core mode when off-resonance and when in resonance with the plasmonic mode. (c) Experimental transmittance for different external refractive indices.

University (Finland) [10] by immersing the sensor into glycerol-water solutions at different concentrations. **Figure 6c** shows the transmittance spectra as a function of the external refractive index. By following the spectral position of the spectral dip, we could measure a sensitivity of 1380 nm/RIU. This sensitivity value is comparable to the ones reported for other plasmonic sensors, which employ fragile fiber tapers and more sophisticated microstructured optical fibers [24, 25]. Thus, we can visualize that the plasmonic sensor based on a gold-coated surface-core fiber is a powerful platform for the realization of highly sensitive refractive index sensing. Moreover, the setup presents the advantages of increased robustness when compared to fragile fiber tapers and simpler preparation than the sensors, which demand metal coating of the inner holes of microstructured fibers.

6. Surface-core fibers for directional curvature sensing

Besides refractive index sensing using Bragg gratings or surface plasmon resonance, surface-core fibers also offer the possibility of the realization of directional curvature sensing. This is possible because the off-center position of the fiber core allows it to experience compression or expansion depending on the curvature direction. In this context, a FBG can be inscribed in the core of the surface-core fiber for probing the bend-induced strain levels inside the core and determine the direction of the curvature.

Compression and expansion of the core introduces strain levels in it. The induced strain in a bent fiber, ε , is proportional to the curvature, C ($\equiv 1/\text{curvature radius}$). If the core is at a distance y from the fiber neutral axis, the induced strain level can be calculated from Eq. (7) [26]. Since the existence of a strain level in a fiber entails variations in its refractive index (by virtue of the strain optic effect) and length, the spectral response of a FBG in this fiber is expected to shift when it is subjected to strain increments. Eq. (8) describes the dependence of the Bragg peak shift as a function of the curvature. In Eq. (8), P_ε is the photoelastic coefficient of silica ($P_\varepsilon = 0.22$) [27].

$$\varepsilon = y C \quad (7)$$

$$\Delta\lambda_B = (1 - P_\varepsilon)\lambda_B\varepsilon = [(1 - P_\varepsilon)\lambda_B y]C \quad (8)$$

To experimentally test the response of the proposed sensor, a FBG was imprinted in the surface-core fiber (by using a phase mask with 1071.2 nm pitch) and the fiber was subjected to curvature increments. The results of the curvature sensing measurements are exposed in **Figure 7**. It is seen that when the fiber experiences expansion, the Bragg peak spectral position redshifts (positive spectral shift). Otherwise, when the fiber is compressed by the bending, the Bragg peak blueshifts (negative spectral shift). The measured sensitivities were (188 ± 5) and (202 ± 5) pm/m⁻¹ for the expansion and compression conditions, respectively.

The achieved sensitivity values are high when compared to other FBG-based sensors whose performance is reported in the literature (sensitivities from 50 to 100 pm/m⁻¹) [28–30]. Additionally, the sensitivity for the surface-core fiber sensor is greater than the one obtained for FBGs sensors in eccentric core polymer optical fibers [31]. It is worth saying, however, that greater sensitivity values can be attained in other configurations. For example, we find in the literature that fibers with two or three cores can provide sensitivities of hundreds of nanometers per inverse meter [32, 33]. Nevertheless, the spectral features whose spectral shifts are considered in [32, 33] are much broader than the Bragg peak in the surface-core fiber we measured. This has an important impact on the sensor resolution. For the

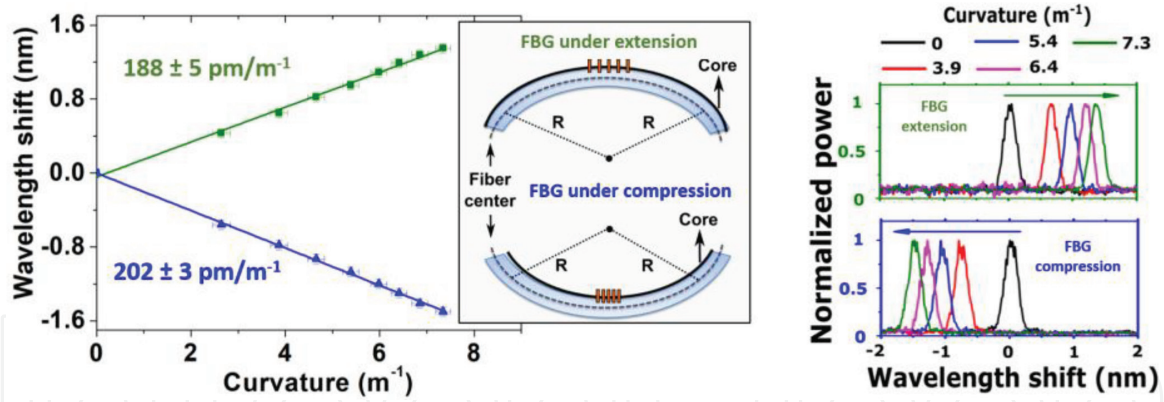


Figure 7.

Wavelength shift as a function of the curvature, representation of the curvature direction and spectral response of the directional curvature sensor based on a FBG inscribed in a surface-core fiber.

sensor reported in [32], for example, one can estimate a resolution limit of 0.01 m^{-1} , which is similar to the one we can find in our results (0.02 m^{-1}).

7. Polymer capillary fibers for temperature sensing

A simpler structure, which can be employed in sensing measurements, is capillary fibers [12]. In our approach, we investigated the sensitivity of polymer capillary fibers to temperature variations by studying the spectral characteristics of the light that is transmitted through its hollow part.

The typical transmission spectra through the hollow part of capillaries have wavelengths of high loss, λ_{\min} . These wavelengths encounter high leakage during propagation because they are resonant with the capillary wall. At these wavelengths, which are given by Eq. (9), transmission minima are observed. In Eq. (9), n_1 is the refractive index of the hollow core, n_2 is the refractive index of the capillary material, d is the thickness of the capillary wall, and m is the order of the minimum. Eq. (9) tells that if the thickness and the refractive index of the capillary are altered, the minima spectral locations are expected to shift. As temperature variations are able to change both these parameters, capillary fibers can act as temperature sensors.

$$\lambda_{\min} = \frac{2n_1d}{m} \sqrt{\left(\frac{n_2}{n_1}\right)^2 - 1} \quad (9)$$

Taking this into account, polymethyl methacrylate (PMMA) capillaries were chosen to be used in this investigation. This decision was due to the high thermal expansion coefficient of PMMA ($2.2 \times 10^{-4} \text{ }^\circ\text{C}^{-1}$) and its high thermo-optic coefficient ($-1.3 \times 10^{-4} \text{ }^\circ\text{C}^{-1}$).

An analytical model can be used to investigate the influences of the thermal expansion and of the thermo-optic effect in the sensor [11, 34]. Eq. (10) presents an expression for calculating the output power (P_{out}) as a function of the wavelength (λ). In Eq. (10), P_{in} is the input power, L is the fiber length, d is the capillary wall thickness, n_1 and n_2 are refractive indexes of the hollow core and of the capillary material, and the parameter Γ is given by Eq. (11). In Eq. (10) and Eq. (11), θ_1 is the angle of incidence of the light rays on the capillary wall for a specific leaky mode—given by $\theta_1 = \sin^{-1}\left(\frac{n_{\text{eff}}}{n_1}\right)$. In the expression for θ_1 , the effective refractive index of the leaky mode guided in the core, n_{eff} , can be found by $n_{\text{eff}} = 1 - \frac{1}{2} \left(\frac{u_{\mu\nu}\lambda}{\pi D_{\text{in}}}\right)^2$,

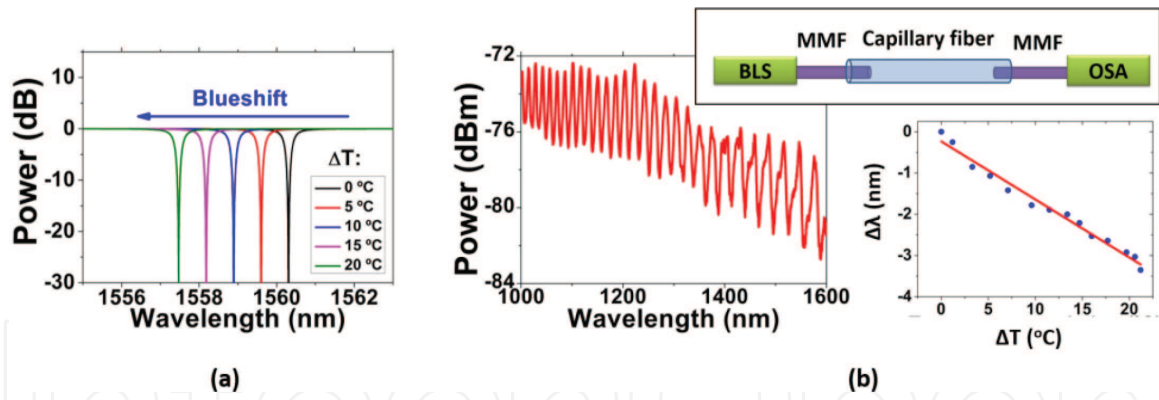


Figure 8. (a) Simulated transmittance of a capillary fiber 2 cm long and with 160 μm inner diameter and 240 μm outer diameter. (b) Experimental transmitted spectrum for a 13 cm long PMMA capillary fiber. Inset stands for the experimental setup (BLS: broadband light source; MMF: multimode fiber; OSA: optical spectrum analyzer) and for the wavelength shift ($\Delta\lambda$) as a function of the temperature variation (ΔT).

where D_{in} is inner diameter of the capillary and $u_{\mu\nu}$ is a root of the equation $J_{\nu-1}(u_{\mu\nu}) = 0$, where J is the Bessel function [34, 35].

$$P_{\text{out}} = P_{\text{in}} \exp \left\{ \left(\frac{L}{D_{\text{in}} \tan \theta_1} \right) \ln \left[1 - \frac{(1 - \Gamma^2)^2}{(1 - \Gamma^2)^2 + 4\Gamma^2 \sin^2 \left(\frac{2\pi n_2 d}{\lambda} \sqrt{1 - \left(\frac{n_1}{n_2} \right)^2 \sin^2 \theta_1} \right)} \right] \right\} \quad (10)$$

$$\Gamma = \frac{\sqrt{1 - \sin^2 \theta_1} - \frac{n_2}{n_1} \sqrt{1 - \left(\frac{n_1}{n_2} \right)^2 \sin^2 \theta_1}}{\sqrt{1 - \sin^2 \theta_1} + \frac{n_2}{n_1} \sqrt{1 - \left(\frac{n_1}{n_2} \right)^2 \sin^2 \theta_1}} \quad (11)$$

Figure 8a presents the simulation for a transmission minimum of a PMMA capillary with 2 cm length, inner diameter 160 μm , and outer diameter 240 μm for different temperature conditions. In the simulation, both thermal expansion and thermo-optic effects are considered. It is seen that, when the temperature increases, the transmission dip is expected to blueshift. It is worth saying that, for the considered capillary fiber, the thermo-optic effect is the dominant effect.

To experimentally test the proposed sensor, a PMMA capillary fiber was fabricated (with inner diameter 160 μm and outer diameter 240 μm) and its performance as a temperature sensor was measured. In the experimental setup, light from a broadband light source was coupled to the capillary fiber (13 cm length) and collected from it by using silica multimode fibers, as shown in the inset of **Figure 8b**. A typical transmission spectrum is shown in **Figure 8b**, and the wavelength shift ($\Delta\lambda$) as a function of the temperature variation (ΔT) is shown in the inset in **Figure 8b**. A sensitivity of (-140 ± 6) pm/ $^\circ\text{C}$ was measured. This sensitivity is around 14 times higher than conventional Bragg gratings-based temperature sensors [36].

8. Conclusions

In this chapter, we presented the recent research yields of our group in the State University of Campinas (Unicamp, Brazil) regarding ultra-simplified

microstructured optical fibers designs for sensing applications. In this context, we firstly discussed hollow and metal-filled embedded-core fibers as pressure and temperature sensors. We showed that the achieved sensitivities with this structure are high when compared to other sensors which employ much more sophisticated fiber designs. Additionally, we described surface-core fibers as refractive index and directional curvature sensors by employing fiber Bragg gratings and a plasmonic configuration. Finally, polymer capillary fibers were presented as an even simpler structure for temperature sensing.

The results presented herein demonstrate the great potential of capillary-like fibers to act as sensors for multiple purposes. Hence, it is possible to identify that this minimalist approach for the design of microstructured fiber sensors consists of a novel and very promising avenue for obtaining sensors with simplified structures and optimized performances.

Acknowledgements

We thank M. A. R. Franco, V. A. Serrão, G. Chesini, S. Aristilde, R. Oliveira, T. H. R. Marques, A. Matikainen, and H. Ludvigsen for their contributions to the development of the research reported herein.

This work was funded by the São Paulo Research Foundation (Fapesp, grant #2014/50632-6), the Financiadora de Estudos e Projetos (Finep, grant #01.12.0393.00), and the National Council for Scientific and Technological Development (CNPq).

Author details

Jonas H. Osório* and Cristiano M. B. Cordeiro
“Gleb Wataghin” Physics Institute, State University of Campinas, Brazil

*Address all correspondence to: cmbc@ifi.unicamp.br

IntechOpen

© 2018 The Author(s). Licensee IntechOpen. This chapter is distributed under the terms of the Creative Commons Attribution License (<http://creativecommons.org/licenses/by/3.0>), which permits unrestricted use, distribution, and reproduction in any medium, provided the original work is properly cited. 

References

- [1] Anuszkiewicz A, Statkiewicz-Barabach G, Borsukowski T, Olszewski J, Martykien T, Urbanczyk W, et al. Sensing characteristics of the rocking filters in microstructured fiber optimized for hydrostatic pressure measurements. *Optics Express*. 2012; **20**(21):23320-23330
- [2] Osório JH, Hayashi JG, Espinel YAV, Franco MAR, Andrés MV, Cordeiro CMB. Photonic-crystal fiber-based pressure sensor for dual environment monitoring. *Applied Optics*. 2014; **53**: 3668-3672
- [3] Kim BH, Lee SH, Lin A, Lee A, Lee J, Han W. Large temperature sensitivity of Sagnac loop interferometer based on the birefringent holey fiber filled with metal indium. *Optics Express*. 2009; **17**: 1789-1794
- [4] Reyes-Vera E, Cordeiro CMB, Torres P. Highly sensitive temperature sensor using a sagnac loop interferometer based on a side-hole photonic crystal fiber filled with metal. *Applied Optics*. 2017; **56**(2):156-162
- [5] Hautakorpi M, Mattinen M, Ludvigsen H. Surface-plasmon-resonance sensor based on three-hole microstructured optical fiber. *Optics Express*. 2008; **16**:8427-8432
- [6] Doherty B, Thiele M, Warren-Smith S, Schartner E, Ebendorff-Heidepriem H, Fritzsche W, et al. Plasmonic nanoparticle-functionalized exposed-core fiber – an optofluidic refractive index sensing platform. *Optics Letters*. 2017; **41**(21):4395-4398
- [7] Osório JH, Chesini G, Serrão VA, Franco MAR, Cordeiro CMB. Simplifying the design of microstructured optical fibre pressure sensors. *Scientific Reports*. 2017; **7**:2990
- [8] Chesini G, Osório JH, Serrão VA, Franco MAR, Cordeiro CMB. Metal-filled embedded-core capillary fibers as highly sensitive temperature sensors. *IEEE Sensors Letters*. 2018; **2**(2)
- [9] Osório JH, Oliveira R, Aristilde S, Chesini G, Franco MAR, Nogueira RN, et al. Bragg gratings in surface-core fibers: refractive index and directional curvature sensing. *Optical Fiber Technology*. 2017; **34**:86-90
- [10] Matikainen A, Osório JH, Nyman M, Juntunen T, Cordeiro CMB, Ludvigsen H. Plasmonic surface-core fibers for high sensitivity refractive index sensing. In preparation
- [11] Osório JH, Marques THR, Figueredo IC, Serrão VA, Franco MAR, Cordeiro CMB. Optical sensing with antiresonant capillary fibers. In: 25th International Conference on Optical Fiber Sensors, Proc. SPIE 10323. 2017. p. 103233U
- [12] Rugeland P, Sterner C, Margulis W. Visible light guidance in silica capillaries by antiresonant reflection. *Optics Express*. 2013; **21**:29217-29222
- [13] Szpulak M, Martykien T, Urbanczyk W. Effects of hydrostatic pressure on phase and group birefringence in microstructured holey fibers. *Applied Optics*. 2004; **43**: 4739-4744
- [14] Primak W, Post D. Photoelastic constants of vitreous silica and its elastic coefficient of refractive index. *Journal of Applied Physics*. 1959; **30**:779
- [15] Timoshenko S, Goodter JN. *Theory of Elasticity*. New York: McGraw-Hill; 1969
- [16] Osório JH, Cordeiro CMB. Optical sensor based on two in-series

birefringent optical fibers. *Applied Optics*. 2013;**52**:4915-4921

[17] Fu HY, Tam HY, Shao L, Dong X, Wai PKA, Lu C, et al. Pressure sensors realized with polarization-maintaining photonic crystal fiber-based Sagnac interferometer. *Applied Optics*. 2008;**47**(15):2835-2839

[18] Martynkien T, Szpulak M, Statkiewicz G, Golojuch G, Olszewski J, Urbanczyk W, et al. Measurements of sensitivity to hydrostatic pressure and temperature in highly birefringent photonic crystal fibers. *Optical and Quantum Electronics*. 2007;**39**:481-489

[19] Martynkien T, Statkiewicz-Barabach G, Olszewski J, Wojcik J, Mergo P, Geernaert T, et al. Highly birefringent microstructured fibers with enhanced sensitivity to hydrostatic pressure. *Optics Express*. 2010;**18**(14):15113-15121

[20] Xin Y, Dong X, Meng Q, Qi F, Zhao C. Alcohol-filled sidehole fiber Sagnac interferometer for temperature measurement. *Sensors and Actuators A: Physical*. 2013;**193**:182-185

[21] Naeem BH, Kim B, Kim YC. High-sensitivity temperature sensor based on a selectively-polymer-filled two-core photonic crystal fiber in-line interferometer. *IEEE Sensors Journal*. 2015;**15**(7):3998-4003

[22] Liang W, Huang Y, Xu Y, Lee RK, Yariv A. Highly sensitive fiber Bragg gratings refractive index sensors. *Applied Physics Letters*. 2005;**86**:151122

[23] Iadicicco I, Cusano A, Cutolo A, Bernini R, Giordano M. Thinned fiber Bragg gratings as high sensitivity refractive index sensor. *Photonics Technology Letters*. 2004;**16**(4):1149-1151

[24] Esteban O, Díaz-Herrera N, Navarrete M, González-Cano A. Surface-plasmon resonance sensors based on uniform-waist tapered fibers in a reflective configuration. *Applied Optics*. 2006;**45**:7294-7298

[25] Hautakorpi M, Mattinen M, Ludvigsen H. Surface-plasmon-resonance sensor based on three-hole microstructured fiber. *Optics Express*. 2008;**16**:8427-8432

[26] Hibbeler RC. *Mechanics of Materials*. 8th ed. Boston: Pearson Prentice Hall; 2011. 978-0-13-602230-5

[27] Kreuzer M. *Strain Measurement with Fiber Bragg Gratings Sensors*. Darmstadt, Germany: HBM; 2006

[28] Gander MG, Mac Pherson WN, McBride R, Jones JDC, Zhang L, Bennion I, et al. Bend measurement using Bragg gratings in multicore fibre. *Electronics Letters*. 2000;**36**(2):120-121

[29] Flockhart GMH, Mac Pherson WN, Barton JS, Jones JDC. Two-axis bend measurement with Bragg gratings in multicore optical fiber. *Optics Letters*. 2003;**28**(6):387-389

[30] Araújo FA, Ferreira LA, Santos JL. Simultaneous determination of curvature, plane of curvature, and temperature by use of a miniaturized sensing head based on fiber Bragg gratings. *Applied Optics*. 2002;**41**(13):2401-2407

[31] Chen X, Zhang C, Webb DJ, Peng G, Kalli K. Bragg grating in a polymer optical fiber for strain, bend and temperature sensing. *Measurement Science and Technology*. 2010;**21**:094005

[32] Villatoro J, Newkirk AV, Antonio-Lopez E, Zubia J, Shülzgen A, Amezcua-Correa R. Ultrasensitive vector bending

sensor based on multicore optical fiber.
Optics Letters. 2016;**41**:832-835

[33] Guzman-Sepulveda JR, May-Arrijo DA. In-fiber directional coupler for high-sensitivity curvature measurement. Optics Express. 2013;**21**: 11853-11861

[34] Lai C, You B, Lu J, Liu T, Peng J, Sun C, et al. Modal characteristics of antiresonant reflecting pipe waveguides for terahertz waveguiding. Optics Express. 2010;**18**(1)

[35] Marcatili EAJ, Schmeltzer RA. Hollow metallic and dielectric waveguides for long distance optical transmission and lasers. The Bell System Technical Journal. 1964;**43**(4)

[36] Oliveira R, Osório JH, Aristilde S, Bilro L, Nogueira RN, Cordeiro CMB. Simultaneous measurement of strain, temperature and refractive index based on multimode interference, fiber tapering and fiber Bragg gratings. Measurement Science and Technology. 2016;**27**:075107

IntechOpen